

Nonlocal Poisson-Fermi double-layer models: Effects of nonuniform ion sizes on double-layer structure

Dexuan Xie*

Department of Mathematical Sciences, University of Wisconsin-Milwaukee, Milwaukee, Wisconsin, 53201-0413, USA

Yi Jiang

Laboratory for Engineering and Scientific Computing, Shenzhen Institutes of Advanced Technology, Chinese Academy of Sciences, Shenzhen 518055, China



(Received 15 August 2017; revised manuscript received 20 February 2018; published 14 May 2018)

This paper reports a nonuniform ionic size nonlocal Poisson-Fermi double-layer model (nuNPF) and a uniform ionic size nonlocal Poisson-Fermi double-layer model (uNPF) for an electrolyte mixture of multiple ionic species, variable voltages on electrodes, and variable induced charges on boundary segments. The finite element solvers of nuNPF and uNPF are developed and applied to typical double-layer tests defined on a rectangular box, a hollow sphere, and a hollow rectangle with a charged post. Numerical results show that nuNPF can significantly improve the quality of the ionic concentrations and electric fields generated from uNPF, implying that the effect of nonuniform ion sizes is a key consideration in modeling the double-layer structure.

DOI: [10.1103/PhysRevE.97.052610](https://doi.org/10.1103/PhysRevE.97.052610)

I. INTRODUCTION

The modeling and simulation of an electric double layer (EDL) has been widely studied in electrochemistry since Helmholtz's early work [1] one century ago, due to its great potential in various important applications, such as water deionization, energy storage and conversion, battery and fuel cell design, and room-temperature ionic liquids. While many EDL models were developed using the classic Poisson-Boltzmann equation (PBE), the ionic size modified PBE (SMPBE), and the Poisson-Fermi equation (PFE) [2–7], most of them were tested only for a rectangular box containing an electrolyte of two ionic species, and solved numerically as two-point boundary value problems under the assumption that all ions have the same volume (or zero volume in the case of PBE), electrodes are planar, and the electrostatic potential on each electrode is a constant.

However, in many applications, a double layer may involve nonplanar electrodes, surface charges on electrodes, more than two ionic species, and distinct ion sizes. A surface potential or a surface charge density on an electrode or a boundary segment may not be a constant. Clearly, incorporating these features of a double layer can significantly improve the current EDL models, but will require new EDL models, new numerical algorithms, and new program packages.

In this paper, we report on a nonuniform ionic size nonlocal Poisson-Fermi double-layer model (nuNPF), a uniform ionic size nonlocal Poisson-Fermi double-layer model (uNPF), and their fast finite element solvers. We then focus on the numerical tests on nuNPF and uNPF for three typical EDL tests defined on a rectangular box, a hollow sphere, and a hollow rectangle

with a charged post. Numerical results show that the effect of nonuniform ion sizes is a key consideration in modeling the double-layer structure with more than two ionic species and large voltages (or large surface charges).

The remaining part of the paper is organized as follows. In Sec. II, we present the nuNPF model and its four special cases: uNPF, a nonuniform SMPBE EDL model (nuSMPBE), a uniform SMPBE EDL model (SMPBE), and a PBE EDL model. In Sec. III, we present the free energy functional that we use to construct nuNPF. In Sec. IV, we present the numerical solvers for nuNPF and uNPF. In Sec. V, we report the numerical test results. Finally, conclusions are made in Sec. VI.

II. OUR ELECTRIC DOUBLE-LAYER MODELS

In this section, we first present the nuNPF EDL model. We then discuss its physical background, and show that it is a family of methods containing uNPF, nuSMPBE, SMPBE, and PBE EDL models as its special cases.

Let D_s be an ionic solvent domain containing n ionic species with charge numbers Z_i , ionic sizes v_i , and bulk concentrations c_i^b of species i , and v_0 be a size scaling parameter. We split the boundary of D_s into two parts, Γ_1 and Γ_2 , to specify the given surface charge σ , voltage g , and other two boundary value functions f_1 and f_2 . See Fig. 1 for an example of D_s . We then define the nuNPF EDL model as a system of $n + 1$ equations, which consists of n nonlinear algebraic equations,

$$c_i - c_i^b \left[1 - \gamma \sum_{j=1}^n v_j c_j \right]^{\frac{v_i}{v_0}} e^{-Z_i u} = 0, \quad i = 1, 2, \dots, n, \quad (1)$$

*dxie@uwm.edu

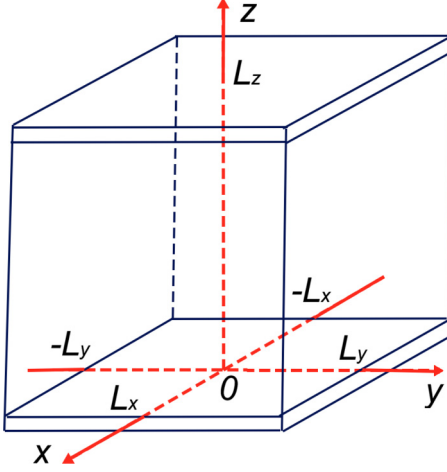


FIG. 1. EDL box with Γ_1 consisting of the four side surfaces and Γ_2 the bottom and top surfaces.

and one nonlocal Poisson-Fermi (NPF) boundary value problem,

$$\begin{cases} -\Delta[u - l_c^2 \Delta u] = \beta \sum_{i=1}^n Z_i c_i & \text{in } D_s, \\ \frac{\partial \Delta u(\mathbf{s})}{\partial \mathbf{n}(\mathbf{s})} = f_1(\mathbf{s}), \quad \frac{\partial u(\mathbf{s})}{\partial \mathbf{n}(\mathbf{s})} = \tau \sigma(\mathbf{s}) & \text{on } \Gamma_1, \\ u(\mathbf{s}) = g(\mathbf{s}), \quad \Delta u(\mathbf{s}) = f_2(\mathbf{s}) & \text{on } \Gamma_2, \end{cases} \quad (2)$$

where u is an electrostatic potential function, c_i is an ionic concentration function of species i , $\gamma = 10^{-27} N_A$, $\Delta = \frac{\partial^2}{\partial x^2} + \frac{\partial^2}{\partial y^2} + \frac{\partial^2}{\partial z^2}$ for $\mathbf{r} = (x, y, z)$, \mathbf{n} is the unit outward normal direction of D_s , $\frac{\partial u(\mathbf{s})}{\partial \mathbf{n}(\mathbf{s})} = \nabla u(\mathbf{s}) \cdot \mathbf{n}(\mathbf{s})$,

$$l_c = \sqrt{\frac{\epsilon_\infty}{\epsilon_s}} \lambda, \quad \beta = \frac{10^{-17} e_c^2 N_A}{\epsilon_0 \epsilon_s k_B T}, \quad \text{and} \quad \tau = \frac{10^{-12} e_c}{\epsilon_0 \epsilon_s k_B T}.$$

Here, ϵ_s and ϵ_∞ are two relative permittivity constants, λ is a parameter for characterizing the spatial frequency of solvent as a dielectric medium, ϵ_0 is the permittivity of the vacuum, e_c is the electron charge, k_B is the Boltzmann constant, T is the absolute temperature, and N_A is the Avogadro constant. In SI units, we have $\gamma \approx 6.0221 \times 10^{-4}$, $\beta \approx 0.05301$, and $\tau \approx 0.0549$ for $\epsilon_s = 80$ and $T = 298.5$. We have measured u in $k_B T / e_c$ (≈ 0.026 volts), c_i and c_i^b in moles per liter (mol/L), σ in $\mu\text{C}/\text{cm}^2$, and the length in angstroms (\AA). Solving the system of nuNPF, we obtain u and the n ionic concentrations c_i simultaneously. We then obtain an electrostatic potential Φ in volts by

$$\Phi = \frac{k_B T}{e_c} u.$$

The nuNPF EDL model is a modification of the nonlocal Poisson-Fermi model reported in Eqs. (36) and (37) of [8]. One major modification is to introduce Neumann and Dirichlet boundary value conditions [in the second and third lines of Eq. (2)] to enable it to work for an EDL with either a surface charge density σ or a voltage g on an electrode. Another

important modification is to remove the concentration function of water molecules and the void volume fraction functions, and then change Eq. (37) in [8] into a new system of Eq. (1). In fact, removing the concentration function of water molecules avoids a redundancy problem since the water solvent has been treated as a continuum dielectric medium. This modification also avoids any void between ionic balls so that the void volume fraction functions become unnecessary. More discussion on the physical insight of nuNPF can be found in the next section.

A related nonlocal Poisson model theory and the physical background of NPF have been well reviewed in [8]. For example, the nonlocal Poisson dielectric model, which is defined in Eq. (8) of [8], is reduced to the classic Poisson dielectric model [see Eq. (5) in [8]] when we set $\epsilon_\infty = \epsilon_s$ or $\lambda = 0$. Thus, it is the biharmonic term $l_c^2 \Delta^2 u$ that takes responsibility for the nonlocal properties of NPF. The source term $\beta \sum_{i=1}^n Z_i c_i$ of the NPF model (2) provides the EDL model with a charge density function for the electrolyte solution. As shown in Eq. (18) of [8], a solution of NPF is the convolution of a solution of a Poisson dielectric model with a Yukawa-like kernel function. In this sense, a solution u of the NPF model (2) can be regarded as a globally ‘‘averaged’’ electrostatic potential over the whole three-dimensional real space.

Our nuNPF EDL model is a family of methods, from which we can obtain four special models as follows: (1) uNPF when all $v_i = v_0$; (2) nuSMPBE when $l_c = 0$; (3) SMPBE when $l_c = 0$ and all $v_i = v_0$; and (4) a PBE double-layer model when $l_c = 0$ and all $v_i = 0$.

In fact, when all $v_i = v_0$, we can find an analytical expression of c_i from Eq. (1) as follows:

$$c_i = \frac{c_i^b e^{-Z_i u}}{1 + \gamma v_0 \sum_{j=1}^n c_j^b e^{-Z_j u}}, \quad i = 1, 2, \dots, n. \quad (3)$$

Substituting the above expressions into Eq. (2), we can obtain uNPF as the nonlinear boundary value problem:

$$\begin{cases} \Delta[u - l_c^2 \Delta u] + \frac{\beta \sum_{i=1}^n Z_i c_i^b e^{-Z_i u}}{1 + \gamma v_0 \sum_{i=1}^n c_i^b e^{-Z_i u}} = 0 & \text{in } D_s, \\ \frac{\partial \Delta u(\mathbf{s})}{\partial \mathbf{n}(\mathbf{s})} = f_1(\mathbf{s}), \quad \frac{\partial u(\mathbf{s})}{\partial \mathbf{n}(\mathbf{s})} = \gamma \sigma(\mathbf{s}) & \text{on } \Gamma_1, \\ u(\mathbf{s}) = g(\mathbf{s}), \quad \Delta u(\mathbf{s}) = f_2(\mathbf{s}) & \text{on } \Gamma_2, \end{cases} \quad (4)$$

where v_0 is set as a water molecule volume (e.g., 3.11^3), or an average volume \bar{v} given by

$$\bar{v} = \frac{1}{n} \sum_{i=1}^n v_i. \quad (5)$$

Setting $l_c = 0$ in Eq. (4) gives SMPBE:

$$\begin{cases} \Delta u + \frac{\beta \sum_{i=1}^n Z_i c_i^b e^{-Z_i u}}{1 + \gamma v_0 \sum_{i=1}^n c_i^b e^{-Z_i u}} = 0 & \text{in } D_s, \\ \frac{\partial u(\mathbf{s})}{\partial \mathbf{n}(\mathbf{s})} = \gamma \sigma(\mathbf{s}) & \text{on } \Gamma_1, \\ u(\mathbf{s}) = g(\mathbf{s}) & \text{on } \Gamma_2, \end{cases} \quad (6)$$

while setting $l_c = 0$ in Eq. (2) gives nuSMPBE as a system of Eq. (1) coupled with the Poisson double-layer model:

$$\begin{cases} -\Delta u = \beta \sum_{i=1}^n Z_i c_i & \text{in } D_s, \\ \frac{\partial u(\mathbf{s})}{\partial \mathbf{n}(\mathbf{s})} = \gamma \sigma(\mathbf{s}) & \text{on } \Gamma_1, \\ u(\mathbf{s}) = g(\mathbf{s}) & \text{on } \Gamma_2. \end{cases} \quad (7)$$

Setting $v_0 = 0$ in the SMPBE model (6) immediately results in the PBE double-layer model:

$$\begin{cases} \Delta u + \beta \sum_{i=1}^n Z_i c_i^b e^{-Z_i u} = 0 & \text{in } D_s, \\ \frac{\partial u(\mathbf{s})}{\partial \mathbf{n}(\mathbf{s})} = \gamma \sigma(\mathbf{s}) & \text{on } \Gamma_1, \\ u(\mathbf{s}) = g(\mathbf{s}) & \text{on } \Gamma_2. \end{cases} \quad (8)$$

When D_s is split into m nonoverlapped subdomains $D_{s,j}$, we define an ion volume occupation rate, V_{ij} , of species i over the j th subdomain $D_{s,j}$ by

$$V_{ij} = \frac{v_i}{|D_{s,j}|} \int_{D_{s,j}} c_i(\mathbf{r}) d\mathbf{r}, \quad i = 1, 2, \dots, n, \quad (9)$$

for $j = 1, 2, \dots, m$. Here $|D_{s,j}|$ denotes the volume of $D_{s,j}$. We then define a total ion occupation rate V_j over $D_{s,j}$ by the formula

$$V_j = \sum_{i=1}^n V_{ij}, \quad j = 1, 2, \dots, m.$$

These rates can be useful in the analysis of ion distributions in the solvent domain D_s for different species. See Figs. 4(e) and 4(f) for examples.

III. OUR FREE ENERGY FUNCTIONAL

We have shown that the ionic concentration $c = (c_1, c_2, \dots, c_n)$ generated from nuNPF is optimal in the sense of minimizing an electrostatic free energy functional as follows:

$$F(c, \tilde{\Phi}) = F_{\text{es}}(c, \tilde{\Phi}) + F_{\text{id}}(c) + F_{\text{ex}}(c), \quad (10)$$

where F_{es} , F_{id} , and F_{ex} are the electrostatic, ideal gas, and excess energies, respectively, in the expressions

$$F_{\text{es}}(c, \tilde{\Phi}) = \frac{k_B T \gamma}{2} \sum_{i=1}^n Z_i \int_{D_s} u(\mathbf{r}) c_i(\mathbf{r}) d\mathbf{r}, \quad (11)$$

$$F_{\text{id}}(c) = k_B T \gamma \sum_{i=1}^n \int_{D_s} c_i \left(\ln \frac{c_i}{c_i^b} - 1 \right) d\mathbf{r}, \quad (12)$$

$$F_{\text{ex}}(c) = \frac{k_B T}{v_0} \int_{D_s} \xi(c) [\ln \xi(c) - 1] d\mathbf{r}. \quad (13)$$

Here $\xi(c) = 1 - \gamma \sum_{i=1}^n v_i c_i(\mathbf{r}) > 0$, which is a volume fraction of the water solution since $\gamma \sum_{i=1}^n v_i c_i(\mathbf{r})$ gives a volume fraction occupied by all the ions.

The free energy F of Eq. (10) is a significant improvement on the conventional free energies used in the derivation of PBE,

SMPBE, and PFE [e.g., see Eq. (4) in [6] or Eq. (36) in [8] for PFE, and Eqs. (1.4) or (3.4) in [9] for SMPBE]. It avoids the drawbacks of the conventional free energies by discarding the thermal de Broglie wavelengths, chemical potentials, a concentration c_0 of water molecules, and terms $\ln(v_i c_i)$.

In detail, our ideal gas term F_{id} of Eq. (12) involves only a given set of bulk concentrations, $\{c_i^b \mid i = 1, 2, \dots, n\}$, and is equivalent to the sum of traditional ideal gas and Gibbs free energy terms, whose definitions involve the thermal de Broglie wavelengths and chemical potentials [10–12]. In fact, using the notation from Eq. (7) of [12], the traditional ideal gas and Gibbs free energy terms f_{id} and f_G are given as

$$f_{\text{id}}(c) = k_B T \sum_{i=1}^n \int_{D_s} c_i(\mathbf{r}) \{ \ln [\Lambda_i^3 c_i(\mathbf{r})] - 1 \} d\mathbf{r},$$

and

$$f_G(c) = - \sum_{i=1}^n \mu_i \int_{D_s} c_i(\mathbf{r}) d\mathbf{r},$$

where Λ_i and μ_i denote the thermal de Broglie wavelength and chemical potential of ionic species i , respectively. The bulk concentration c_i^b is then found as

$$c_i^b = \Lambda_i^{-3} e^{\mu_i / (k_B T)}, \quad i = 1, 2, \dots, n.$$

Using the above expression, we can obtain the chemical potential μ_i in the expression

$$\mu_i = k_B T \ln (c_i^b \Lambda_i^3), \quad i = 1, 2, \dots, n,$$

and then simplify the sum of $F_{\text{id}}(c)$ and $F_G(c)$ as

$$f_{\text{id}}(c) + f_G(c) = k_B T \sum_{i=1}^n \int_{D_s} c_i \left(\ln \frac{c_i}{c_i^b} - 1 \right) d\mathbf{r}.$$

When ionic concentrations are measured in moles per liter, we multiply the scale parameter $\gamma = 10^{-27} N_A$ on both sides of the above identity to yield our ideal gas free energy term of Eq. (12). This shows the equivalence of our free energy functional to the traditional one without considering any ionic size effect (the PBE case).

In our term F_{ex} of Eq. (13), we used the size scaling parameter v_0 instead of the water molecule concentration c_0 . This modification avoids a redundancy problem caused by using c_0 since the water solution has been treated as a continuum dielectric. We also observe that using c_0 causes voids among ions and water molecules, breaking down the size constraint condition

$$\xi(c) + \gamma \sum_{i=1}^n v_i c_i(\mathbf{r}) = 1, \quad \mathbf{r} \in D_s.$$

In addition, the terms $\ln(v_i c_i)$ used in a conventional excess energy term become undefined at $v_i = 0$ so that the case of PBE is excluded as a special case in the conventional free energy functional for SMPBE and NPF.

IV. NUMERICAL SOLVERS

We developed finite element iterative algorithms and software packages for solving nuNPF and uNPF based on our PBE

and SMPBE program packages [13–15], and the state-of-the-art finite element library from the FEniCS project [16]. In our algorithms, we constructed a Lagrange finite element function space \mathcal{M} as a subspace of the usual Sobolev space $H^1(D_s)$ using a tetrahedral mesh of D_s , and a finite element vector function space $\mathcal{N}_1 \times \mathcal{N}_2$. We then introduced an additional function, ψ , to reformulate Eq. (2) as a variational form as follows:

Find $(u, \psi) \in \mathcal{N}_1 \times \mathcal{N}_2$ such that

$$\begin{aligned} & \int_{D_s} \nabla u \cdot \nabla v_1 d\mathbf{r} + \int_{D_s} \psi v_1 d\mathbf{r} + l_c^2 \int_{D_s} \nabla \psi \cdot \nabla v_2 d\mathbf{r} \\ & + \int_{D_s} \psi v_2 d\mathbf{r} \\ & = -\beta \int_{D_s} v_2 \sum_{i=1}^n Z_i c_i d\mathbf{r} + \tau \int_{\Gamma_1} \sigma v_1 ds \\ & + l_c^2 \int_{\Gamma_1} f_1 v_2 ds \quad \forall (v_1, v_2) \in \mathcal{N}_0 \times \mathcal{N}_0, \end{aligned} \quad (14)$$

where $\mathcal{N}_0 = \{v \in \mathcal{M} \mid v = 0 \text{ on } \Gamma_2\}$, $\mathcal{N}_1 = \{v \in \mathcal{M} \mid v = g \text{ on } \Gamma_2\}$, and $\mathcal{N}_2 = \{v \in \mathcal{M} \mid v = f_2 \text{ on } \Gamma_2\}$. Let $u^{(k)}$ and $c_i^{(k)}$ denote the k th iterative approximations to u and c_i for $i = 1, 2, \dots, n$, and $\xi(c^{(k,k+1)})$ be defined by

$$\xi(c^{(k,k+1)}) = 1 - \gamma \left(\sum_{j=1}^{i-1} v_j c_j^{(k+1)} + \sum_{j=i}^n v_j c_j^{(k)} \right).$$

In the nuNPF iterative scheme, uNPF is used to generate initial iterates $u^{(0)}$ and $c_i^{(0)}$ for $i = 1, 2, \dots, n$. When both $u^{(k)}$ and $c_i^{(k)}$ are known, the $(k+1)$ th iterates $c_i^{(k+1)}$ for $i = 1, 2, \dots, n$ are defined by the recursive formulas:

$$c_i^{(k+1)} = c_i^{(k)} - \omega \frac{c_i^{(k)} - c_i^b e^{-Z_i u^{(k)}} [\xi(c^{(k,k+1)})]^{v_i/v_0}}{1 + \gamma \frac{v_i^2}{v_0} c_i^b e^{-Z_i u^{(k)}} [\xi(c^{(k,k+1)})]^{v_i/v_0 - 1}},$$

and the $(k+1)$ th iterate $u^{(k+1)}$ is then defined by

$$u^{(k+1)} = u^{(k)} + \omega[\bar{u} - u^{(k)}],$$

where ω is a relaxation parameter between 0 and 2, and \bar{u} denotes a solution of the linear variational problem: Find $(u, \psi) \in \mathcal{N}_1 \times \mathcal{N}_2$ such that

$$\begin{aligned} & \int_{D_s} \nabla u \cdot \nabla v_1 d\mathbf{r} + \int_{D_s} \psi v_1 d\mathbf{r} + l_c^2 \int_{D_s} \nabla \psi \cdot \nabla v_2 d\mathbf{r} \\ & + \int_{D_s} \psi v_2 d\mathbf{r} \\ & = -\beta \int_{D_s} v_2 \sum_{i=1}^n Z_i c_i^{(k+1)} d\mathbf{r} + \tau \int_{\Gamma_1} \sigma v_1 ds \\ & + l_c^2 \int_{\Gamma_1} f_1 v_2 ds \quad \forall (v_1, v_2) \in \mathcal{N}_0 \times \mathcal{N}_0. \end{aligned}$$

The iteration is terminated when $u^{(k+1)}$ and $c_i^{(k+1)}$ satisfy

$$\max \left\{ \|u^{(k+1)} - u^{(k)}\|, \max_{1 \leq i \leq n} \|c_i^{(k+1)} - c_i^{(k)}\| \right\} < \epsilon,$$

where ϵ is a convergence tolerance ($\epsilon = 10^{-5}$ by default). Our program packages work for any number of ionic species.

Note that the problem for solving \bar{u} is a system of linear algebraic equations with the coefficient matrix independent of iterations. Hence, one efficient scheme for solving it is the LU factorization method in which the coefficient matrix is factorized as a lower triangular matrix (L) and an upper triangular matrix (U) (see Sec. 3.2 in [17]). In implementation, the LU factorization is carried out only once before starting the iteration. At each iteration, we only need to solve one lower triangular linear system and one upper triangular linear system, resulting in a very fast iterative scheme.

V. NUMERICAL TESTS

We made numerical experiments on nuNPF and uNPF to show the effect of nonuniform ion sizes on the structure of the double layer. In these tests, each ion of species i was treated as a ball with radius a_i so that the volume $v_i = \frac{4\pi}{3} a_i^3$. The values of a_i (in Å) were selected as the radii of hydrated ions from [18]: 3.58, 4.12, 3.32, 3.31, and 3.35 for Na^+ , Ca^{+2} , Cl^- , K^+ , and NO_3^- , respectively. For simplicity, we set $f_1 = f_2 = 0$, $\epsilon_s = 80$, $\epsilon_\infty = 1.8$, $T = 298.5$, and $\lambda = 15$ for all the tests. In the tests for nuNPF, we set $v_0 = \min_{1 \leq i \leq n} v_i$.

For clarity, we present the numerical results in five sections. In Sec. VA, we did tests for an EDL electrolyte solution domain D_s being a box of Fig. 1 to compare the application range and accuracy of nuNPF with that of uNPF, SMPBE, nuSMPBE, and PBE, and to demonstrate the importance of considering nonuniform ion sizes in EDL modeling under a strong electrostatic field. In Sec. VB, we did tests using a hollow sphere of Fig. 2 as D_s to demonstrate how the co-ions (such as Na^+ and K^+) compete with each other for space near a highly charged spherical surface to further show the importance of considering nonuniform ion sizes in EDL modeling. In Sec. VC, we did tests for D_s being a hollow rectangle of Fig. 5(a) with a charge density function $\sigma(x, y)$ on the inner circle to demonstrate the significant effects of nonuniform ion sizes on the electric field of an EDL. Finally, comparison tests with molecular dynamic and Monte Carlo simulation data were done in Secs. VD and VE, respectively, as initial validation tests for our new models.

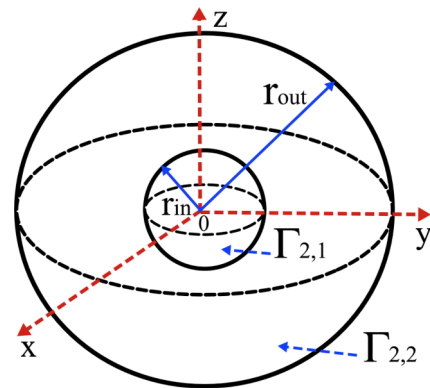


FIG. 2. Hollow sphere with $\Gamma_2 = \Gamma_{2,1} \cup \Gamma_{2,2}$ and $\Gamma_1 = \emptyset$. Here $\Gamma_{2,1}$ and $\Gamma_{2,2}$ denote the inner and outer spherical surfaces with radii r_{in} and r_{out} , respectively.

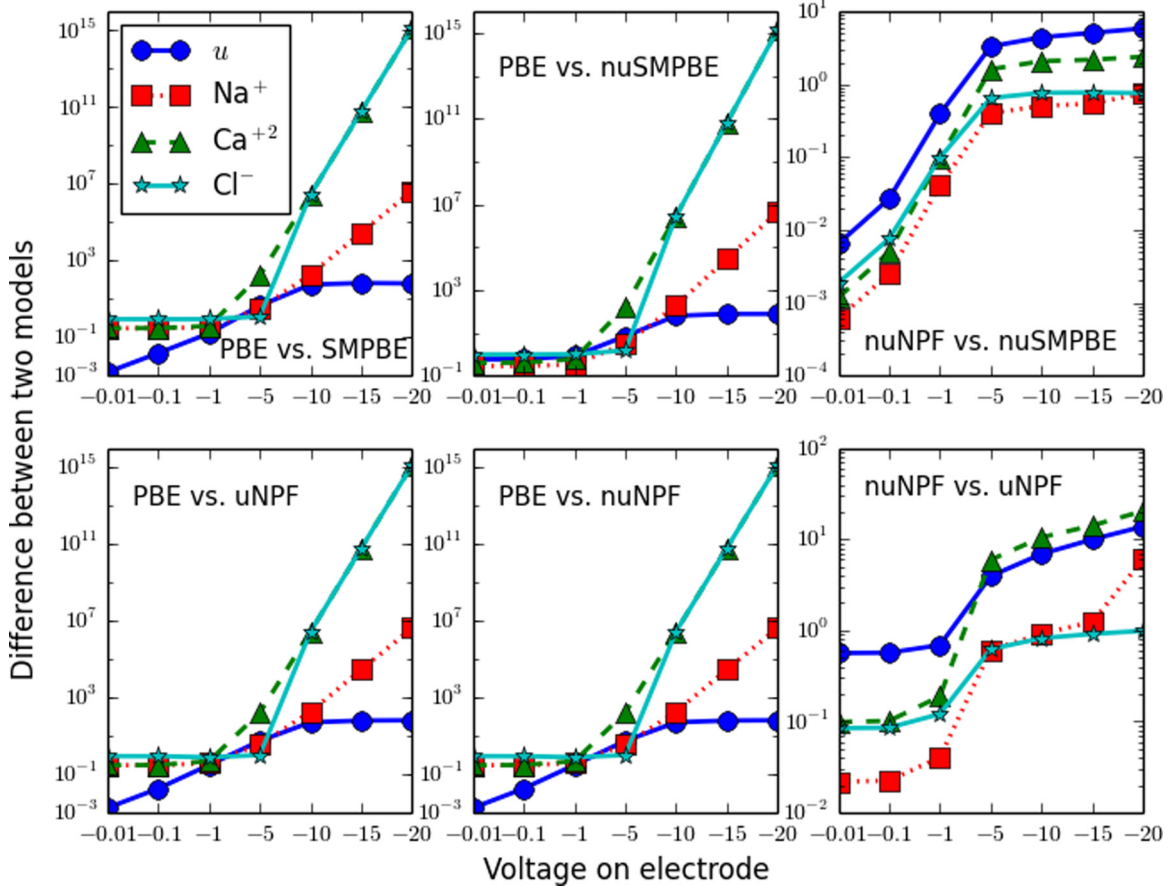


FIG. 3. Differences between two models defined in Eq. (15) for the EDL tests on a box of Fig. 1.

A. Tests for EDL with a box domain

In these tests, a rectangular box D_s , as illustrated in Fig. 1, was set with $L_x = L_y = 10$ and $L_z = 50$ (in Å). Γ_1 included the four side surfaces of the box, and Γ_2 included the bottom and top surfaces. The box D_s contained a mixture of Na^+ , Ca^{+2} , and Cl^- with $Z_1 = +1$ and $c_1^b = 0.1$ for Na^+ , $Z_2 = +2$ and $c_2^b = 0.1$ for Ca^{+2} , and $Z_3 = -1$ and $c_3^b = 0.3$ for Cl^- . The voltage function $g = 0$ on the top surface (one EDL electrode) at $z = L_z$, and the surface charge density $\sigma = 0$ on Γ_1 were set for all the tests.

We first did tests on nuNPF for this EDL using $g = -0.01, -0.1, -1, -5, -10, -15$, or -20 on the bottom surface of the box D_s (the other electrode of EDL) at $z = 0$ in order to check the validity range and accuracy of nuNPF. As comparison, we also solved uNPF, nuSMPBE, SMPBE, and PBE for these EDL cases. All the tests were done by using a cubic finite element method on an interval $0 \leq z \leq L_z$ due to the symmetry of the EDL model. We then calculated the differences between two models in the L_2 -norm $\|\cdot\|_{L_2(D_s)}$ as follows:

$$\|u_a - u_b\|_{L_2(D_s)}, \quad \|c_{i,a} - c_{i,b}\|_{L_2(D_s)}, \quad i = 1, 2, 3, \quad (15)$$

where $u_a, u_b, c_{i,a}$, and $c_{i,b}$ denote the electrostatic potentials and ionic concentrations calculated by models a and b from the nuNPF, uNPF, nuSMPBE, SMPBE, and PBE EDL models, and $\|\cdot\|_{L_2(D_s)}$ is defined by $\|v\|_{L_2(D_s)} = \sqrt{\int_{D_s} |v|^2 d\mathbf{r}}$ for v in the function space $L_2(D_s)$. These differences were plotted as functions of the voltage g in Fig. 3.

Figure 3 shows that the differences between any two models were small for a low voltage of g (e.g., $|g| < 1$ in these tests), implying that PBE or SMPBE would be good enough. But, for a high voltage (e.g., $|g| > 5$), the differences became significant, even huge, so a sophisticated EDL model like nuNPF becomes necessary in the study of EDL structures in ionic concentrations.

We next tested nuNPF with a high voltage, $g = -30$, on the electrode at $z = 0$ and kept D_s as a box for the purpose of confirming the symmetry of the EDL model. In these tests, we solved nuNPF and uNPF by a linear finite element method on a uniform mesh of D_s with mesh size $h = 0.5$. We also calculated the ion occupation rates V_{ij} of Eq. (9), where the interval $0 \leq z \leq 50$ was divided into six and seven equal segments for uNPF and nuNPF, respectively, to fit each ion ball, since the largest ion ball in nuNPF, a calcium ion ball, has radius 4.12, and each ion ball in uNPF has radius 3.7 since we set $v_0 = \bar{v}$. Here \bar{v} is defined in Eq. (5).

All the grid values of the concentrations of Na^+ , Ca^{+2} , and Cl^- from the box mesh were plotted in points, resulting in three curves in Fig. 4(a) for uNPF and Fig. 4(b) for nuNPF. This well validates the symmetry property of the EDL box model; both u and c_i vary only along the z -axis direction. Hence, this confirms that the EDL box model can be solved equivalently as a two-point boundary value problem for $0 \leq z \leq L_z$ as done mostly in the current literature.

Figures 4(a) and 4(b) show that uNPF and nuNPF had very different concentrations for Na^+ and Ca^{+2} . The ion

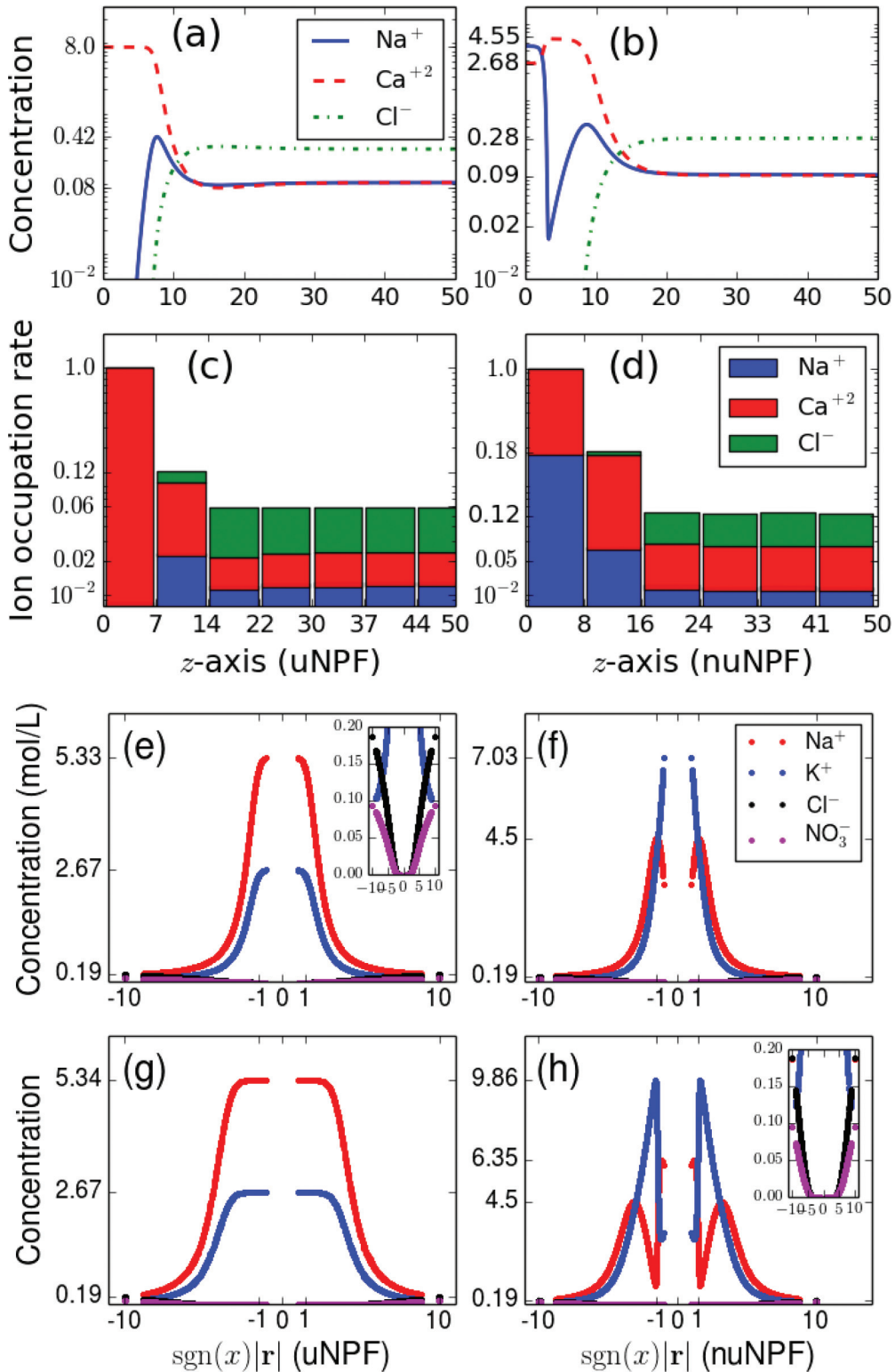


FIG. 4. (a, b) A comparison of the concentrations of uNPF with that of nuNPF for a box of Fig. 1 using a mixture of Na^+ , Ca^{+2} , and Cl^- . (c, d) A further comparison in the ion concentration rates V_{ij} of Eq. (9). (e, f) A comparison of the concentrations of uNPF with that of nuNPF for a hollow sphere of Fig. 2 using a mixture of Na^+ , K^+ , Cl^- , and NO_3^- and voltage -10 . (g, h) A further comparison for the hollow sphere using voltage -30 .

occupation rates V_{ij} of Eq. (9) produced by uNPF and nuNPF were reported in Figs. 4(c) and 4(d), from which it can be seen that while both uNPF and nuNPF produced the Stern layer (the first ion occupation bar) and the dif-

fuse layer (the other bars), nuNPF modified the Stern layer of uNPF sharply from a layer of pure calcium ions to a mixed layer of calcium (about 80%) and sodium (about 20%) ions.

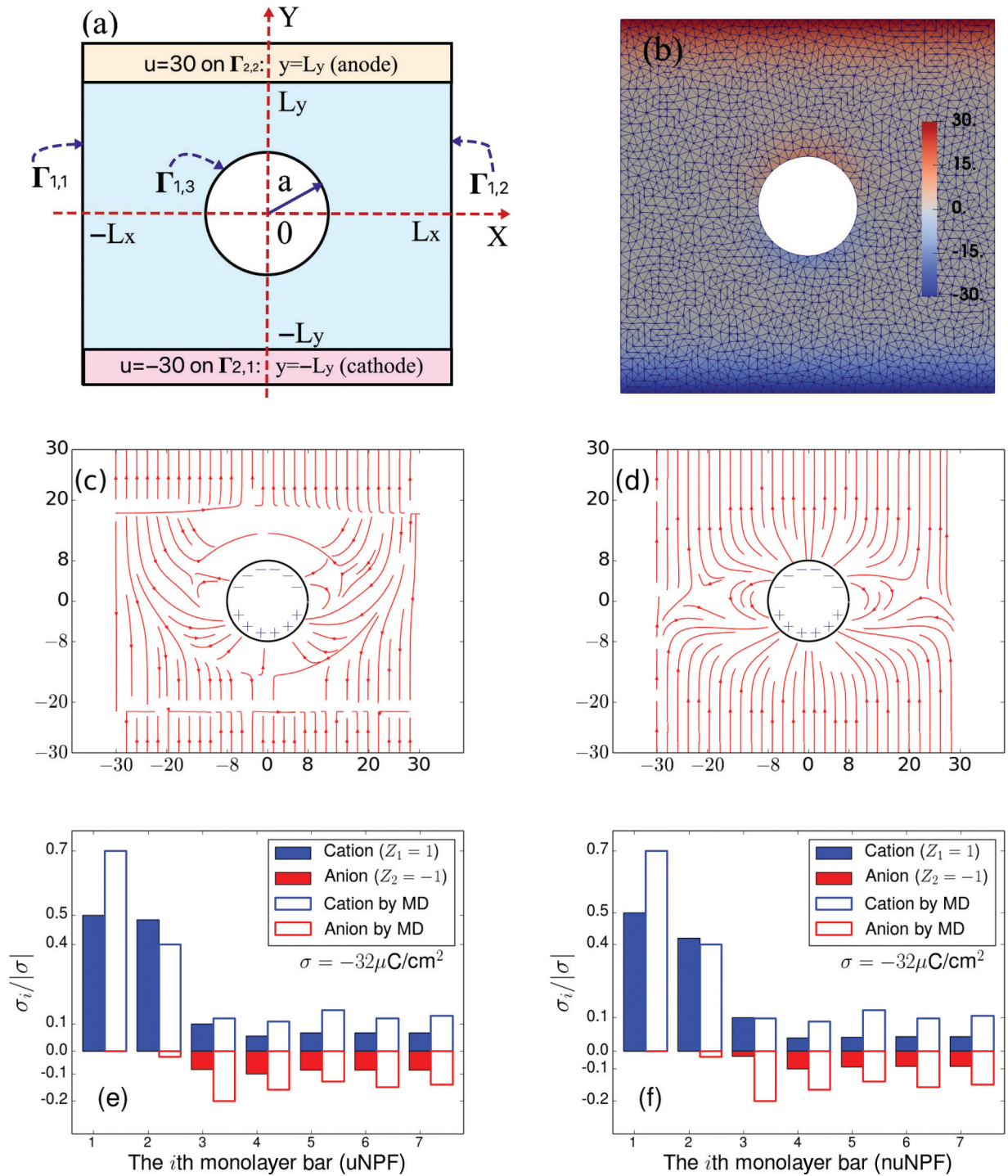


FIG. 5. (a) Hollow rectangle with $L_x = L_y = 30$ and a charge function, $\sigma(x, y) = -8y$, on the inner circle $\Gamma_{1,3}$ with radius $a = 8$. (b) Electrostatic potential u by nuNPF mapped onto the mesh in colors. (c) Electric field ∇u by uNPF. (d) Electric field ∇u by nuNPF. (e, f) Comparison of uNPF and nuNPF with an EDL molecular dynamics (MD) simulation [20] on the box domain of Fig. 1. Here $\sigma_i = \int_{10^{i-1}}^{10^i} c_j(z) dz$ for $i = 1$ to 7 , $j = 1, 2$.

These tests indicate that near a strongly negatively charged electrode, for cations in the same size, the one with the higher charge is more successful in vying for space, but for cations in different sizes, smaller ions can become more successful. Hence, the consideration of nonuniform ion sizes is important in the double-layer modeling.

B. Tests for EDL with a hollow sphere domain

In these tests, we set D_s as a hollow sphere, $D_s = \{\mathbf{r} | \mathbf{r}_{in} < |\mathbf{r}| < \mathbf{r}_{out}\}$, as illustrated in Fig. 2, with $\mathbf{r}_{in} = 1$ and $\mathbf{r}_{out} = 10$ for a mixture of four ionic species with $Z_1 = +1$ and $c_1^b = 0.2$ for Na^+ , $Z_2 = +1$ and $c_2^b = 0.1$ for K^+ , $Z_3 = -1$ and $c_3^b = 0.2$ for Cl^- , and $Z_4 = -1$ and $c_4^b = 0.1$ for NO_3^- . In this

case, the inner and outer spherical surfaces $\Gamma_{2,1}$ and $\Gamma_{2,2}$ are two electrodes with $g = -10$ (or -30) and $g = 0$, respectively, $\Gamma_2 = \Gamma_{2,1} \cup \Gamma_{2,2}$, and $\Gamma_1 = \emptyset$. We solved nuNPF and the uNPF using $v_0 = \bar{v}$ via a quadratic finite element method on an irregular tetrahedral mesh of D_s with 18 662 mesh points. We plotted the concentrations of Cl^- and NO_3^- in two insets on Figs. 4(e) and 4(h) due to their small values.

Figures 4(e)–4(h) show that the Na^+ and K^+ concentrations of uNPF were sharply changed when the ion ball radii of Na^+ and K^+ were changed from the same value to distinct values. Near the negatively charged electrode, for cations with the same size and charge number, the ion with a larger bulk concentration has a larger concentration [the case of uNPF as shown in Figs. 4(e) and 4(g)]. But, when their hydrated radii are different, the ionic species with a smaller size can produce a larger concentration even with a smaller bulk concentration [the case of nuNPF as shown in Figs. 4(f) and 4(h)]. These test results further indicate the importance of the consideration of nonuniform ion sizes.

C. Tests for EDL with a hollow rectangle domain

In these tests, we set a hollow rectangle domain D_s , as illustrated in Fig. 5(a), to mimic an induced electro-osmosis around a metal post (Fig. 1 in [19]). Here, $L_x = L_y = 30$, $a = 8$, $\sigma = 0$ on $\Gamma_{1,1}$ and $\Gamma_{1,2}$, $g = -30$ on $\Gamma_{2,1}$, $g = 30$ on $\Gamma_{2,2}$, and an induced charge density function, $\sigma(x, y) = -8y$, on $\Gamma_{1,3}$ (a circle with radius $a = 8$), whose extreme and neutral values ($\pm 64 \mu\text{C}/\text{cm}^2$ and 0) were reached at points $(0, \pm a)$ and $(\pm a, 0)$, respectively. We solved the uNPF using $v_0 = 3.11^3$ and nuNPF for a mixture of Na^+ , Ca^{+2} , and Cl^- , as set in Sec. V A, via a cubic finite element method on a triangular mesh with 1935 vertices, as shown in Fig. 5(b), where the electrostatic potential u generated by nuNPF has been mapped onto the mesh domain in colors. We then calculated the electric fields $-\nabla u$ generated by uNPF and nuNPF, and plotted them in streamlines in Figs. 5(c) and 5(d).

Figures 5(c) and 5(d) show that nuNPF and uNPF produced very different electric fields. The uNPF field had many broken streamlines. Surprisingly, it was modified sharply to the one with the streamlines that follow the rules of electrostatics when the distinct ion sizes were retrieved. This indicates that the effect of nonuniform ion sizes has a critical impact even on the electric field of an electric double layer.

D. Comparison tests with MD simulation data

While the test results of Secs. V A–V C demonstrate the importance of nonuniform ion size effects on EDL structures, it is interesting to compare nuNPF and uNPF with an ionic liquid molecular dynamic (MD) test done in [20]. In this MD test, 1050 cations ($Z_1 = +1$) and 1050 anions ($Z_2 = -1$) were added to the box of Fig. 1 with $L_x = L_y = 55$ and $L_z = 450$, which gave the bulk concentrations

$$c_j^b = 1050 / (110^2 \times 450) 10^{27} / N_A \approx 0.32 \text{ mol/L}, \quad j = 1, 2,$$

$\sigma = -32$ on the electrode at $z = 0$, $\sigma = 32$ on the other electrode at $z = 450$, and each ion was treated as a ball with radius 5 \AA . Because of the symmetry, we solved this EDL as

a two-point mixed boundary value problem for $0 \leq z \leq 225$ with the boundary value conditions

$$\frac{du(0)}{dz} = -32, \quad u(225) = 0.$$

In uNPF, we set $v_0 = 10^3$, which is about a volume of a ball with radius 6.2. Thus, in nuNPF, the radii of cations and anions were set as 6.2 and 3.1, respectively. We set $\epsilon_s = 15$ to get $u \approx -102$ at $z = 0$, which is close to the value of 100 used in [6], and retained all the other parameter values including $T = 298.5$ (a room temperature) instead of $T = 450$ used in [6,20].

Following the MD simulation report in [20], we displayed the distributions of cations and anions predicted by uNPF and nuNPF near the electrode at $z = 0$ in the bar plots of Figs. 5(e) and 5(f). Here, the distributions were split into seven consecutive layers, each bar represents one layer, and the width of each bar was set as the diameter (10 \AA) of an ionic ball. For comparison, we also plotted the MD data in Figs. 5(e) and 5(f).

From Figs. 5(e) and 5(f) it can be seen that both uNPF and nuNPF produced two layers of cations near the electrode, which agree with the MD case. While the first two layers of uNPF reached the maximal admissible value of ionic concentration, nuNPF had only one layer that did so, which is similar to the MD data. This difference between uNPF and nuNPF indicates the effects of nonuniform ion sizes on an EDL of an ionic liquid. Similar to the MD case, both uNPF and nuNPF also predicted that the most cations were collected to the first two layers so that the other five layers had weak oscillations.

E. Comparison tests with MC simulation data

Monte Carlo (MC) simulation techniques were applied to the study of EDL for monovalent, divalent, symmetric, or asymmetric electrolytes for a low voltage of g (e.g., $|g| < 1$) or a weakly surface charge. As comparisons, we did tests on nuNPF for an EDL case studied by MC techniques in [21]. In these tests, the domain D_s was set as the box of Fig. 1

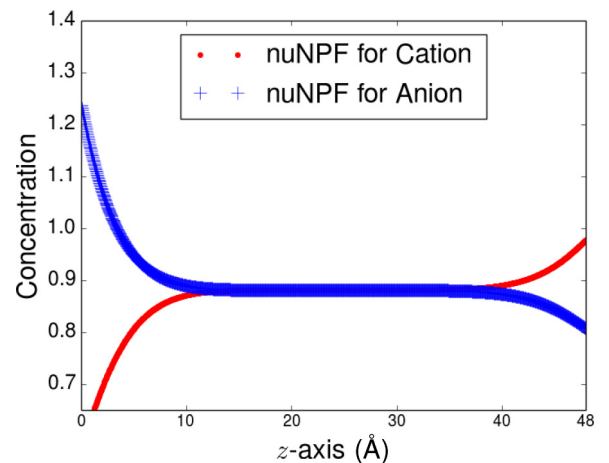


FIG. 6. Concentrations C_1 and C_2 of cations and anions produced by nuNPF for the EDL case in Fig. 9 of [21]. Here $C_1(z) = C_2(z) = 0.88$ for $13 \leq z \leq 35$.

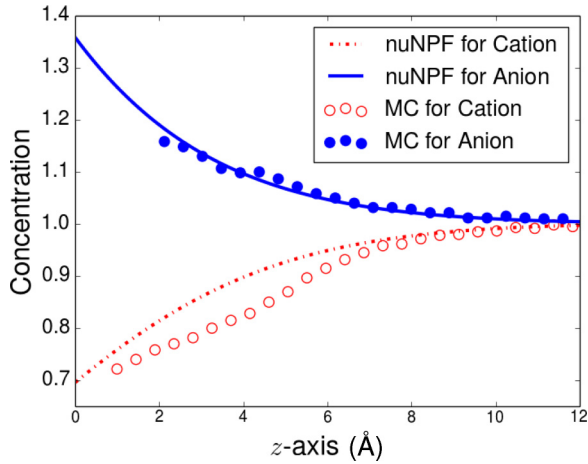


FIG. 7. Comparison of the ionic concentrations calculated by nuNPF with the Monte Carlo (MC) simulation data reported in [21].

containing a 1:1 electrolyte, the radii of cations and anions were set as 1 Å and 2.125 Å, respectively (i.e., $n = 2$, $Z_1 = 1$, $Z_2 = -1$, $a_1 = 1$, and $a_2 = 2.125$), and the bulk concentrations were set as $c_1^b = c_2^b = 1$ mol/L. In our tests, we kept these data and other default parameters for simplicity while setting $L_z = 48$, $\sigma = 2\mu\text{C}/\text{cm}^2$ at $z = 0$, and $u = 0$ at $z = 48$ Å. The length $L_z = 48$ was found to be long enough to reveal an electro-neutrality region, which was about $13 \leq z \leq 35$. In such a region, the concentrations c_i are expected to equal the bulk concentrations c_i^b . Hence, we define c_i by

$$c_i(z) = C_i(z) + [c_i^b - C_i(L_z/2)], \quad 0 \leq z \leq L_z, \quad i = 1, 2,$$

where C_i denotes the i th ionic concentration calculated by nuNPF. The values of C_i are displayed in Fig. 6, from which it was found that $C_i(L_z/2) \approx 0.88$. Thus, we got $c_i = C_i + 0.12$ for $i = 1, 2$, and plotted them in Fig. 7, along with the MC data from Fig. 9 of [21].

Figure 7 shows that the nuNPF results agree well with the MC data. Furthermore, we repeated the tests via the uNPF and SMPBE using $a_1 = a_2 = 1$ Å, and $a_1 = a_2 = 2.125$ Å, respectively. Their results were found very similar to those produced by nuNPF due to a low voltage g at $z = 0$ (about 0.5). This further confirms the observations we derived from Fig. 3. In the case of low voltages, we prefer SMPBE and uNPF to nuNPF due to their simplicity and efficiency in calculation even though nuNPF can work as well as uNPF and SMPBE.

VI. CONCLUSIONS

In summary, we have reported on the two electric double-layer models, nuNPF and uNPF, as well as their special cases: nuSMPBE, SMPBE, and PBE. We then developed the finite element algorithms and software packages for solving these EDL models. This work enables us to calculate EDL structures for more than two ionic species, nonuniform ion sizes, variable surface charges, and nonplanar electrodes in three-dimensional space. We also introduced a free energy functional as a significant improvement on the conventional free energies used in the derivation of PBE, SMPBE, and PFE. Moreover, we show that the nuNPF EDL model can predict the EDL structure in terms of ionic concentrations optimally in the sense of minimizing the free energy functional.

Using our nuNPF program package, we performed three typical EDL tests, as reported in Secs. VA–VC, for up to four ionic species and high concentrations up to about 10 mole/L. The test results demonstrate how the cations with different sizes (such as a pair of Na^+ and Ca^{+2} with the same bulk concentration or a pair of Na^+ and K^+ with different bulk concentrations) compete with each other for space in the vicinity of a highly negatively charged surface. They confirm that the effect of nonuniform ion sizes is a key consideration in the prediction of the structure of EDL models under a strong electrostatic field. The importance of ion size effects is known in EDL modeling and simulation, but here it has been confirmed computationally via a dielectric continuum model, our nuNPF model, for a three-dimensional EDL with more than two ionic species.

Furthermore, we compared uNPF and nuNPF with molecular dynamics and Monte Carlo simulation data, as well as the nuSMPBE, SMPBE, and PBE EDL models. These test results demonstrate the validity range and accuracy of our models. In the future, we plan to further explore the accuracy, performance, and application of nuNPF and uNPF, and validate nuNPF and uNPF using more EDL molecular dynamic and Monte Carlo simulation data from the literature (e.g., the Granada group's work reported in [22]). We also will use our new software packages to simulate various EDL applications that are difficult to study with current simulation techniques for a mixture solution containing a number of ionic species in different ion sizes and an electrode with a high voltage or a strong surface charge density. Such simulations are expected to yield insight into the structure of EDL and to further improve our nuNPF EDL model.

- [1] H. v. Helmholtz, Ueber einige gesetze der vertheilung elektrischer ströme in körperlichen leitern mit anwendung auf die thierisch-elektrischen versuche, *Ann. Phys. (NY)* **165**, 211 (1853).
- [2] M. S Kilic, M. Z Bazant, and A. Ajdari, Steric effects in the dynamics of electrolytes at large applied voltages. I. Double-layer charging, *Phys. Rev. E* **75**, 021502 (2007).
- [3] M. Z Bazant, M. S Kilic, B. D Storey, and A. Ajdari, Towards an understanding of induced-charge electrokinetics at large applied voltages in concentrated solutions, *Adv. Colloid Interface Sci.* **152**, 48 (2009).
- [4] A. C. Maggs and R. Podgornik, General theory of asymmetric steric interactions in electrostatic double layers, *Soft Matter* **12**, 1219 (2016).
- [5] P. M. Biesheuvel and M. Van Soestbergen, Counterion volume effects in mixed electrical double layers, *J. Colloid Interface Sci.* **316**, 490 (2007).
- [6] M. Z. Bazant, B. D. Storey, and A. A. Kornyshev, Double Layer in Ionic Liquids: Overscreening Versus Crowding, *Phys. Rev. Lett.* **106**, 046102 (2011).
- [7] A. A. Kornyshev, Double-layer in ionic liquids: Paradigm change? *J. Phys. Chem. B* **111**, 5545 (2007).

- [8] D. Xie, J. L. Liu, and B. Eisenberg, Nonlocal Poisson-Fermi model for ionic solvent, *Phys. Rev. E* **94**, 012114 (2016).
- [9] B. Li, Continuum electrostatics for ionic solutions with non-uniform ionic sizes, *Nonlinearity* **22**, 811 (2009).
- [10] F. Fogolari and J. M. Briggs, On the variational approach to Poisson-Boltzmann free energies, *Chem. Phys. Lett.* **281**, 135 (1997).
- [11] J. Che, J. Dzubiella, B. Li, and J. A. McCammon, Electrostatic free energy and its variations in implicit solvent models, *J. Phys. Chem. B* **112**, 3058 (2008).
- [12] D. Xie and J. Li, A new analysis of electrostatic free energy minimization and Poisson-Boltzmann equation for protein in ionic solvent, *Nonlinear Anal. Real World Appl.* **21**, 185 (2015).
- [13] D. Xie, New solution decomposition and minimization schemes for Poisson-Boltzmann equation in calculation of biomolecular electrostatics, *J. Comput. Phys.* **275**, 294 (2014).
- [14] Y. Xie, J. Ying, and D. Xie, SMPBS: Web server for computing biomolecular electrostatics using finite element solvers of size modified Poisson-Boltzmann equation, *J. Comput. Chem.* **38**, 541 (2017).
- [15] D. Xie, New finite element iterative methods for solving a nonuniform ionic size modified Poisson-Boltzmann equation, *Int. J. Numer. Anal. Model.* **14**, 688 (2017).
- [16] Edited by A. Logg, K.-A. Mardal, and G. N. Wells, *Automated Solution of Differential Equations by the Finite Element Method*, Lecture Notes in Comput. Sci. Eng., Vol. 84 (Springer-Verlag, Berlin, 2012).
- [17] G. H. Golub and C. F. van Loan, *Matrix Computations*, 3rd ed. (Johns Hopkins University, Baltimore, 1996).
- [18] E. R. Nightingale Jr., Phenomenological theory of ion solvation. effective radii of hydrated ions, *J. Phys. Chem.* **63**, 1381 (1959).
- [19] M. Z. Bazant and T. M. Squires, Induced-Charge Electrokinetic Phenomena: Theory and Microfluidic Applications, *Phys. Rev. Lett.* **92**, 066101 (2004).
- [20] M. V. Fedorov and A. A. Kornyshev, Towards understanding the structure and capacitance of electrical double layer in ionic liquids, *Electrochim. Acta* **53**, 6835 (2008).
- [21] M. Valisko, D. Henderson, and D. Boda, Competition between the effects of asymmetries in ion diameters and charges in an electrical double layer studied by Monte Carlo simulations and theories, *J. Phys. Chem. B* **108**, 16548 (2004).
- [22] G. I. Guerrero-García, E. González-Tovar, M. Quesada-Pérez, and A. Martín-Molina, The non-dominance of counterions in charge-asymmetric electrolytes: Non-monotonic precedence of electrostatic screening and local inversion of the electric field by multivalent coions, *Phys. Chem. Chem. Phys.* **18**, 21852 (2016).